Analyst

RSC Publishing

PAPER

View Article Online
View Journal | View Issue

Cite this: *Analyst*, 2013, **138**, 4607

High performance optical sensing nanocomposites for low and ultra-low oxygen concentrations using phase-shift measurements†

Santiago Medina-Rodríguez,*[ab] Marta Marín-Suárez,[b] Jorge Fernando Fernández-Sánchez,*[b] Ángel de la Torre-Vega,[a] Etienne Baranoff[c] and Alberto Fernández-Gutiérrez[b]

The accurate and real-time measurement of low and ultra-low concentrations of oxygen using non-invasive methods is a necessity for a multitude of applications, from brewing beer to developing encapsulating barriers for optoelectronic devices. Current optical methods and sensing materials often lack the necessary sensitivity, signal intensity, or stability for practical applications. In this report we present a new optical sensing nanocomposite resulting in an outstanding overall performance when combined with the phase-shift measurement method (determination of luminescence lifetime in the frequency domain). For the first time we have incorporated the standard PtTFPP dye (PtTFPP = platinum(II) 5,10,15,20-meso-tetrakis-(2,3,4,5,6-pentafluorophenyl)-porphyrin) into AP200/19, a nanostructured aluminium oxide-hydroxide solid support. This sensing film shows an excellent sensitivity between 0 and 1% O_2 (K_{SV} = 3102 ± 132 bar^{-1}) and between 0 and 10% O_2 (K_{SV} = 2568 ± 614 bar^{-1}) as well as $\Delta\tau_{0.05\%}$ (62.53 ± 3.66%), which makes it 62 times more sensitive than PtTFPP immobilized in polystyrene and also 8 times more sensitive than PtTFPP immobilized on silica beads. Furthermore the phase-shift measurement method results in a significant improvement (about 23 times) in stability compared to the use of intensity recording methods. The film also displays full reversibility, long shelf stability (no change observed after 12 months), and it is not affected by humidity. To establish this sensing methodology and develop sensors over the full range of the visible light, we also studied three other dye-AP200/19 nanocomposites based on phosphorescent cyclometalated iridium(III) complexes.

Received 31st January 2013
Accepted 7th May 2013

DOI: 10.1039/c3an00239j

www.rsc.org/analyst

Introduction

In recent years there has been considerable interest and tremendous research activity in the field of chemical sensing for real-time monitoring of analytes (CO_2, O_2, *etc.*) and properties (pH, temperature, *etc.*).[1,2] Molecular oxygen is one of the most important analytes in our environment as it is widely involved in a variety of chemical and biochemical reactions both as a reactant and as a product. Although the detection of oxygen is well known in principle, this area continues to attract sustained attention. New methods, new oxygen sensing materials, and new sensors with improved performance have been developed in the last two decades to detect oxygen in both gas and liquid phases.[3–12] Clark electrodes and Winkler titration are widely used methods to quantify oxygen. However, these two methods are both invasive and destructive. Consequently optical sensors have gained particular interest in recent years as a non-invasive, non-destructive measurement method.

Optical sensors are particularly attractive due to the absence of electromagnetic interferences, their high sensitivity and resolution, and null oxygen consumption. In addition, the versatility of formats (planar, nanoparticles, paints, optical fibers, *etc.*), the possibility of miniaturization, and the suitability for 2D and 3D imaging have also encouraged their utilization.[13] They also provide a wireless readout, fast response, as well as non-invasive, real-time monitoring in remote, hazardous, or *in vivo* environments.[4] For these reasons, optical sensors have become very popular in many fields related to industry, medicine, biotechnology, and environment.[8,14–23]

[a]*Department of Signal Theory, Networking and Communications, CITIC-UGR, University of Granada, C/Periodista Rafael Gómez 2, E-18071 Granada, Spain. E-mail: smedina@ugr.es; Fax: +34 958243328; Tel: +34 958 240451*

[b]*Department of Analytical Chemistry, Faculty of Sciences, University of Granada, Avda. Fuentenueva s/n, E-18071 Granada, Spain. E-mail: jffernan@ugr.es*

[c]*School of Chemistry, University of Birmingham, Edgbaston, B15 2TT, England, UK*

† Electronic supplementary information (ESI) available: Chemical structures of the dyes, full details about the homemade oxygen sensing characterization system, fundamentals of oxygen sensing measured by the phase-resolved method (frequency domain), full details of characterization of the oxygen-sensing films, additional figures for the oxygen sensitivity of the iridium(III) complexes, and additional tables including the data measured. See DOI: 10.1039/c3an00239j

However, current optical methods and sensing materials often lack the necessary sensitivity, signal intensity, or stability for practical applications. Furthermore, most of them are optimized for detecting physiological concentrations and are less suitable for low oxygen concentrations.[13] Sensing of oxygen traces is of great interest in many areas of science and technology; for example, oxygen trace sensing has become crucial in microbiology, since a variety of microorganisms grow under special conditions, from low levels of residual oxygen to anaerobic conditions.[24] Oxygen trace sensing also has special application in the control of modified atmosphere packaging (MAP), where an adequate oxygen concentration is required inside the package in order to maintain the microbiological stability of fresh-cut fruits and vegetables, by limiting aerobic respiration without inducing anaerobic processes.[25] In addition, oxygen trace control is important for avoiding discoloration, browning and softening of these products, where oxygen concentrations typically below 0.25–5 kPa are required.[26–28]

The development of an oxygen-sensitive sensor requires (1) a luminescent dye, the luminescence of which changes with the oxygen concentration; (2) a solid support in which the dye can be immobilized; (3) a signal transduction system, which correlates the luminescent changes with the oxygen concentration.

Optical oxygen sensors have previously been demonstrated with numerous luminescent dyes.[3,8,9,29–33] Iridium(III) organometallic complexes have been widely used due to their high luminescence quantum yields, high photostability, long decay times (luminescence lifetimes), strong absorption bands, large Stokes' shift, fast response time and high Stern–Volmer constants.[3,29,30,33,34] Platinum(II) and palladium(II) porphyrin complexes are also very successful materials for optical sensing of low and ultra-low oxygen concentrations.[13,35–38] In this paper, four organometallic complexes (one of Pt(II) and three of Ir(III)) have been used as oxygen-sensitive dyes.

The solid support is an important component of an oxygen sensor as it impacts the sensing ability mainly in two ways:[29] first by the permeability to oxygen, which enables fast diffusion of oxygen to the emitting molecules for quenching; second by their chemical nature, which leads to different aggregation behaviors of the dyes resulting in different accessibility of oxygen. Ideally, a matrix must be permeable to oxygen, should be structurally stable enough to withstand mechanical stress, and should increase photostability.[33] In addition, it has to prevent the leaching and migration of chemical compounds by insulation of the dyes and has to preclude the aggregation of the dye.[11] In this paper, a nanostructured inorganic (aluminium oxide-hydroxide; AlOOH) solid support has been selected due to its excellent properties for the aforementioned requirements.[29,30,34,39,40]

Most optical methods for measuring the oxygen concentration are based on recording changes in emission intensity or luminescence lifetime.[19,20,22,41–44] Unfortunately, while intensity measurements are relatively simple and accurate in the laboratory,[30,43,45] they are often inadequate in real-world applications because the emission intensity is highly influenced by external perturbations.[43,46] These difficulties can be minimized by measuring the luminescence lifetime.[43,47] The luminescence lifetime can be measured either in the time domain (time-resolved method) or in the frequency domain (phase-resolved method).[4] Although time-resolved methods are ideally suited for the elimination of the background luminescence and scattering,[4] high-speed photodetectors and specific signal processing devices are required, which makes this approach rather expensive. On the other hand, frequency-domain lifetime measurement does not generally require much sophisticated instrumentation,[22,46] and allows for the use of simple and cheap light sources and electronic devices.[43,48] Thus, a phase-resolved method is usually preferred for the design of robust and reliable sensors, and was employed in this work.

To sum up, in this work four organometallic complexes immobilized into a nanostructured AlOOH solid support have been characterized by a phase-resolved method for the determination of low and ultra-low oxygen concentrations. To the best of our knowledge, this is the first time that this type of sensing material has been characterized by luminescence lifetime in the frequency domain. In addition, it is the first time that the PtTFPP complex has been immobilized into a nanostructured AlOOH solid support. Combining the intrinsic properties of PtTFPP (long lifetime of the excited state, good stability and excellent photochemical properties), the properties that the immobilization into a nanostructured solid support provide (increase of the sensitivity to oxygen and decrease of the response time), and the phase-shift measurement method (increase in resolution and stability), we developed one of the best candidates for ultra-low oxygen-sensitive films which has good luminescence signal intensity, excellent sensitivity, complete reversibility, exceptional stability, and is not affected by humidity. Finally the use of phosphorescent cyclometalated iridium(III) complexes with various emission wavelengths allowed us to establish this sensing methodology and develop sensors over the full range of colors of the visible spectrum.

Experimental details

Materials and chemicals

Platinum(II) 5,10,15,20-meso-tetrakis-(2,3,4,5,6-pentafluorophenyl)-porphyrin, named PtTFPP, was obtained from Frontier Scientific (http://www.frontiersci.com). Iridium(III) complexes [Ir(2-(2,4-difluorophenyl)pyridine)$_2$(4,4′-dimethylamino-2,2′-bipyridine)]-(PF_6), named N969, [Ir(2-(2,4-difluorophenyl)pyridine)$_2$(4,7-diphenyl-1,10-phenanthroline)](PF_6), named N1008, and [Ir(2-(2,4-difluoro-3-methylesterphenyl)pyridine)$_2$(4-(*N*,*N*-dimethylamino)picolinate)], named EB146, were synthesized as described in the literature.[29,30,49] ESI shows the chemical structure of these oxygen-sensitive dyes (see Fig. ESI-1†).

The nanostructured material was prepared by Ilford Imaging Switzerland following the procedure previously published.[34,39] It is called AP200/19, and it is based on a thin plate of polyethylene terephthalate (PET) coated with a thin layer of aluminium oxide hydroxide (AlOOH), which provides a positively charged nanostructured film with a pore diameter of 19 nm and a total pore volume of 20 mL m^{-2}.[30]

Chloroform was obtained from Fluka (http://www.sigmaaldrich.com), which was used as an organic solvent due to its good properties to dissolve the dyes. Nitrogen and oxygen

(all of 99.999% purity) were obtained from Air Liquide (http://www.airliquide.com).

Preparation of the oxygen-sensing films

The cocktails were prepared by dissolving PtTFPP, N969, N1008 or EB146 in 2 mL of chloroform (dye concentration of 1.5 mg mL^{-1}). The cocktails were shaken on an IKA-Vibramax-VXR (IKA-Labortechnik, Staufen, Germany) until the dye was completely dissolved. The oxygen-sensitive membranes were obtained using a Laurell spin-coater (WS-400B-6NPP/LITE, Laurell Technologies, http://www.laurell.com, North Wales, PA, USA). 100 μL of the cocktail were injected onto the rotating metal oxide support fixed onto a spinning device at 300 rpm. AP200/19 membranes obtained after the deposition process were translucent and allowed some visible light to pass through them. Three replicas for each membrane were prepared in order to evaluate the error. All the experimental results were expressed as the average of 3 replicas ± error ($s \cdot t/\sqrt{n}$), were s is the standard deviation, t is the Student's t, and n is the number of replicas.

Instruments and methods

Excitation and emission spectra were acquired on a Varian Cary-Eclipse luminescence spectrometer (Varian Inc.-Agilent Technologies, http://www.agilent.com, CA, USA) equipped with a Xe flash lamp (peak power equivalent to 75 kW), Czerny-Turner monochromators, and a red-sensitive photomultiplier tube (PMT) R-928 from Hamamatsu Photonics (http://www.sales.hamamatsu.com, Japan) with manual or automatic voltage regulator.

The control of oxygen and lifetime measurements was carried out with a homemade system (see details in the ESI†). Details about the fundamentals of oxygen sensing measured by the phase-resolved method (frequency domain) and about the characterization of the oxygen-sensing films are given in the ESI.†

Results and discussion

Photophysical properties of the nanocomposites

Four different oxygen-sensing films have been evaluated. They are based on the immobilization of one Pt(II) (PtTFPP) and three Ir(III) (N969, N1008 and EB146) oxygen-sensitive dyes into an inorganic nanostructured matrix (AP200/19).

PtTFPP was selected because it is one of the most popular and widely used oxygen-sensitive luminescent dyes for the preparation of optical oxygen sensors.[44] It is primarily due to its excellent photostability, rapid response times, high sensitivity at low oxygen concentrations, and strong phosphorescence at room temperature (*i.e.*, high photoluminescence quantum yield).[13,32,50]

N969, N1008 and EB146 were selected to cover a large variety of properties, such as a wide range of emission wavelengths, high quantum yield, and an expected high sensitivity to low oxygen concentrations, according to previous studies developed by our research group.[29,30] This range of properties make them interesting not only for controlling residual oxygen or anaerobic conditions (*i.e.*, as optical trace oxygen sensors), but also in applications that require different excitation and/or emission wavelengths and sensitivities (case of multi-parameter optical sensors).[6,51–55]

Table 1 Maxima luminescence excitation and emission wavelengths ($\lambda_{exc/em}$) and luminescence lifetime in the absence of oxygen (τ_0) of the dyes incorporated into AP200/19. [Dye concentration] = 1.5 mg mL^{-1} and monochromator slit-width$_{exc/em}$ = 10/10 nm

Dye	λ_{exc} (nm)	λ_{em} (nm)	τ_0 (μs)
PtTFPP	395	650	97.25 ± 3.21
N969	350	490	3.74 ± 0.02
N1008	340	512	8.40 ± 0.07
EB146	335	470	1.88 ± 0.01

Table 1 shows the luminescence excitation and emission properties of the different sensing films, as well as their

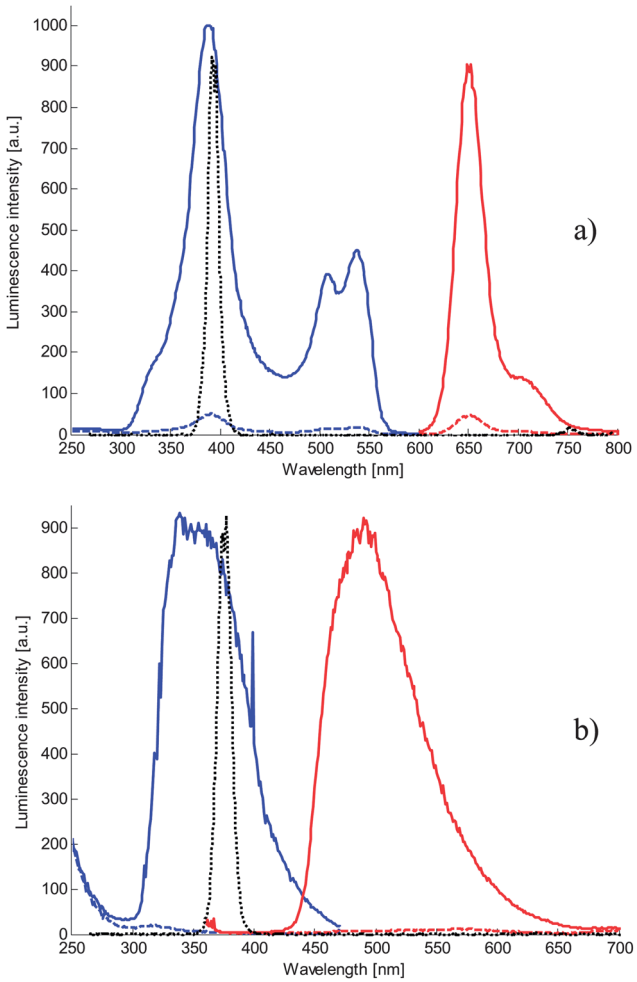

Fig. 1 Excitation (blue lines) and emission (red lines) spectra of the dyes in the absence (solid lines) and in the presence (dashed lines) of oxygen of (a) PtTFPP and (b) N969 immobilized into AP200/19. The black dotted line (···) is the emission spectra of the LED used to excite the sensing film. [Dye] = 1.5 mg mL^{-1}, λ_{exc} = 389 nm for PtTFPP and 350 nm for N969, λ_{em} = 650 nm for PtTFPP and 490 nm for N696, slit-width$_{exc/em}$ = 10/10 nm, delay time = 0.1 ms, gate time = 5 ms, detector voltage = 440 V for PtTFPP and 590 V for N969, flow-rate 200 mL min^{-1}.

luminescence lifetimes in the absence of oxygen and at 21 °C. Fig. 1 shows the luminescence excitation and emission spectra in the absence and in the presence of oxygen (100% N_2 and 100% O_2, respectively) of PtTFPP and N969 (as a representative Ir(III) complex) immobilized into AP200/19; the spectra of the other two Ir(III) complexes are similar to those of N969 and they are shown in the ESI (see Fig. ESI-3†). In all cases, the emission was clearly quenched when the sensing films were exposed to oxygen. In addition, Fig. 1 also shows the emission spectra of both LEDs used for exciting the dyes. The Ir(III) complexes immobilized into AP200/19 can be efficiently excited in the near ultraviolet range (320–380 nm), showing good compatibility with the selected ultraviolet 375 nm LED, and PtTFPP immobilized into AP200/19 can be excited in the Soret band (380–400), thus the selected ultraviolet 395 nm LED is optimum for the excitation of this sensing film.

The maximal luminescence excitation and emission wavelengths of PtTFPP immobilized into AP200/19 are similar to the maxima obtained for this dye incorporated into a classical polystyrene membrane,[43,51] chemically attached to silica beads,[13] and in solution.[56] Thus, the incorporation of PtTFPP into AP200/19 does not affect its emission spectrum. Interestingly, the luminescence lifetime (τ_0) for PtTFPP immobilized into AP200/19 ($\simeq$97 μs) is higher than the same dye dissolved in polystyrene ($\simeq$55 μs)[32] and chemically immobilized in silica beads ($\simeq$71 μs).[13] It could be due to the high efficiency of incorporation into the nanopores of the nanostructured aluminum oxide which reduces the probability of radiationless excited state deactivation.[34,40]

The incorporation of N969, N1008 and EB146 into AP200/19 has been previously analyzed.[29,30] The incorporation of N969 and N1008 into the nanostructured material provides a shift in their excitation and emission wavelengths compared with those in solution. It was attributed to the ionic nature of these complexes; they are positively charged with negatively charged counterions and therefore possibly interact strongly with the positively charge metal oxide.[30] On the other hand, the immobilization of EB146 into AP200/19 does not affect its luminescence properties because it is a neutral complex.[29]

Selection of the modulation frequency

The phase-based lifetime measurement at a fixed frequency requires the choice of an optimal modulation frequency for a given measurement range of oxygen.[43,57] In this case, measurement intervals between 0 and 1% O_2 and between 0 and 10% O_2 were chosen as the measurement ranges of interest to calibrate the oxygen-sensitive films. In order to select the most appropriate value of the modulation frequency of each sensing film at a given oxygen range, the average phase-shift differences between 0 and 1% O_2 ($|\phi_{0\%} - \phi_{1\%}|$) and between 0 and 10% O_2 ($|\phi_{0\%} - \phi_{10\%}|$) within a certain range of modulation frequencies (from 100 Hz to 98 kHz, the maximum operating frequency available for the commercial dual-phase lock-in amplifier) were determined.

A simple and powerful methodology based on a multifrequency phase-resolved method (referred to as multifrequency I/Q method and developed by our research group)[43] was used to detect the oxygen-concentration-dependent phase-shift simultaneously at multiple modulation frequencies (see ESI, Fig. ESI-4 and Table ESI-1†). Multifrequency signals composed of 16 sinusoids of different frequencies were used to find the most appropriate value of the modulation frequency for each sensing film. This frequency was defined as the lowest modulation frequency giving the highest $|\phi_{0\%} - \phi_{x\%}|$. This multifrequency method significantly reduces the measurement time required to find the modulation frequency of a sensing film, providing similar results to those obtained with the well-known commercial dual-phase lock-in amplifier operating at a single frequency (see Fig. ESI-5 and Tables ESI-2 to ESI-5†).

This study concludes that the most suitable modulation frequencies (in the frequency range 100 Hz–98 kHz) for the measurement range 0–10% O_2 are 94 100 Hz for the sensing films containing N969 (average phase difference of 32.97°) and EB146 (average phase difference of 28.41°), 30 100 Hz for the sensing film containing N1008 (average phase difference of 24.59°) and 40 100 Hz (average phase difference of 53.20°) for the sensing film containing PtTFPP. Similar modulation frequencies were obtained for the measurement range 0–1% O_2.

Oxygen-sensitive properties

All the membranes under study were evaluated with the setup described in Fig. ESI-2,† and phase-shift measurements were obtained for several oxygen concentrations. Fig. 2 shows the variation of the phase shift of PtTFPP and N969 incorporated into AP200/19 when they are exposed to various concentrations of oxygen; ESI shows the phase shift variation for the other sensing films under study (see Fig. ESI-6†) and the values obtained for all the measurements (see Tables ESI-6 to ESI-13†). Using eqn ESI-4,† we determined the lifetimes and therefore the Stern–Volmer plots (τ_0/τ *versus* oxygen concentration) of all membranes. Fig. 3 shows the calibration curves and the Stern–Volmer plots of the four oxygen-sensitive films along the fitting according to Demas Model (equation ESI-2†). Table 2 summarizes the fitting parameters.

Data in Table 2 show that the most sensitive sensing film is PtTFPP immobilized into AP200/19, which has K_{SV1} of 3102 bar^{-1} in the range 0–1% O_2 and K_{SV1} of 2568 bar^{-1} in the range 0–10% O_2

To compare with a more classical membrane for detecting O_2, the PtTFPP was immobilized into a polystyrene (PS) support and measured with the same setup and under the same conditions (from 0 to 10% pO_2) at its optimal modulation frequency (5145 Hz).[43] In this case, the data have to be fitted with the Lehrer method (see equation ESI-3 in the ESI†). PtTFPP immobilized into PS shows the following results: $x_0 = 0.846 \pm 0.005$, $K_{SV} = 41.42 \pm 0.87$ bar^{-1}. The incorporation of PtTFPP into AP200/19 increases its sensitivity more than 62 times referenced to PS. Furthermore, the Stern–Volmer constant between 0 and 1% O_2 of PtTFPP chemically attached to silica beads is 423 bar^{-1} and chemically attached to silica beads in silicone is 370 bar^{-1}.[13] The incorporation of PtTFPP into AP200/19 increases the sensitivity more than 8 times compared to

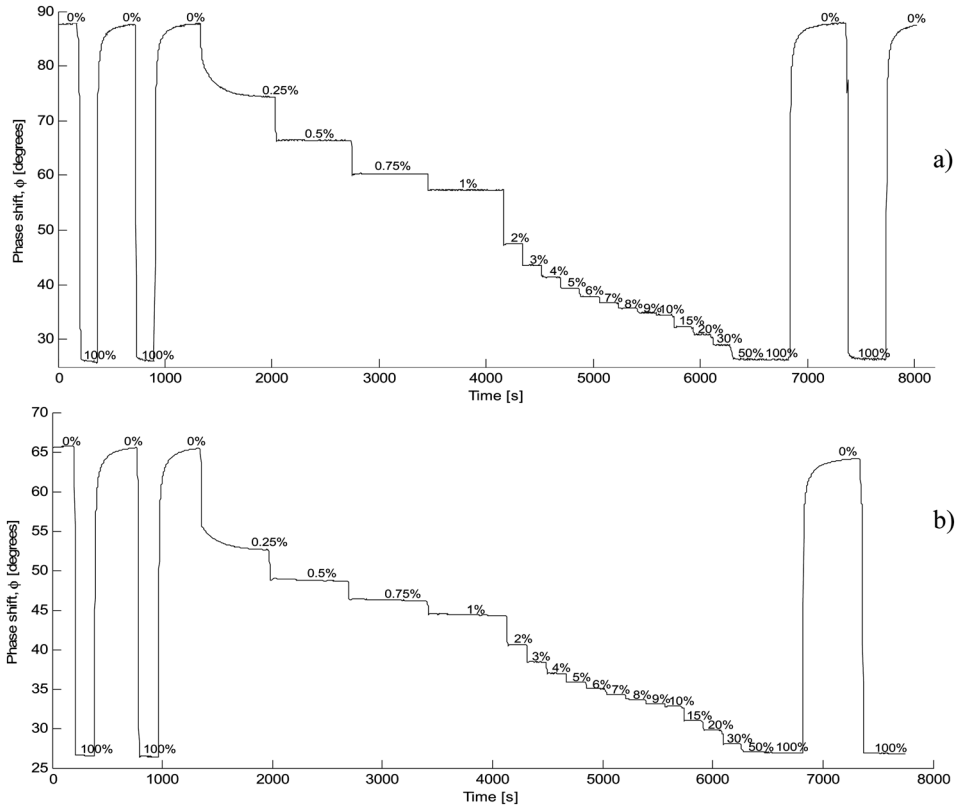

Fig. 2 Variation of the phase shift of (a) PtTFPP and (b) N969 incorporated into AP200/19 with the oxygen concentration.

silica beads. This interesting increase of sensitivity has been previously described for Ru(II) and Ir(III) complexes, but is demonstrated for the first time for a Pt(II) complex.

Concerning the Ir(III) complexes immobilized into AP200/19, the highest sensitivity for low oxygen concentrations is obtained for N969. It shows a K_{SV1} of 941 bar^{-1} in the range 0–1% O_2, which is about 23 times higher than the K_{SV1} of PtTFPP incorporated into PS and more than 2 times higher than the K_{SV1} of PtTFPP incorporated into silica beads, even when its luminescence lifetime is more than 18 times lower. Therefore, N969 incorporated into AP200/19 is an alternative of Pt(II) complex for oxygen trace sensing.

By comparing these results with other sensing membranes described in the literature,[13,32,51] PtTFPP immobilized into AP200/19 is one of the most sensitive sensing layers developed to date. Only two oxygen-sensitive sensing films are more sensitive. The first one is based on fullerene C_{70} incorporated into ethylcellulose. It shows a K_{SV} of 70 000 bar^{-1},[58] 22 times higher than PtTFPP in AP200/19 from 0 to 1% O_2, but this dye shows low luminescence brightness at RT and high temperature dependence of lifetime and sensitivity.[13] The second one consists of PdTFPP chemically immobilized in silica-beads in silicone and shows a K_{SV} of 6700 bar^{-1} from 0 to 0.1% O_2 (ref. 13) that is twice more than PtTFPP in AP200/19 from 0 to 1% O_2; it should be noted that the available data for PdFTPP are for a range 0–0.1% O_2 while the data obtained for PtTFPP are from 0 to 1% O_2. The high sensitivity of PdTFPP is due to its long luminescence lifetime; therefore it is anticipated that its sensitivity would also increase if this dye is immobilized in AP200/19. On the other hand, the sensitivity of PdTFPP and PtTFPP sensing layers has low temperature dependence and both dyes are highly photostable.

In order to demonstrate that the developed sensing films can also be used for ultra-low oxygen detection the gas station was modified by replacing the pure oxygen with synthetic air (mixture of oxygen and nitrogen). With this new setup, the minimum oxygen concentration achievable is 0.05% pO_2. ESI (see Tables ESI-14 to ESI-21†) shows the phase shift and luminescence lifetime variations for all the measurements between 0 and 0.26% pO_2 and a summary of the results is shown in Fig. 4, which demonstrates that all the membranes can be used for detecting ultra-low oxygen concentrations.

To determine the most sensitive membrane for concentrations lower than 0.05% pO_2, $\Delta\tau_{0.05\%}$ was determined. $\Delta\tau_{0.05\%}$ is defined as the percentage of the luminescence lifetime quenched at 0.05% oxygen and is a rough guide to the sensitivity of the optical oxygen sensing films. It was calculated according to eqn (1):

$$\Delta\tau_{0.05\%} = \frac{\tau_0 - \tau_{0.05}}{\tau_0 - \tau_{100}} \times 100 \quad (1)$$

where τ_0 corresponds to the luminescence lifetime in the absence of oxygen, $\tau_{0.05}$ is the luminescence lifetime in the presence of 0.0005 bar (0.05%) oxygen and τ_{100} is the luminescence lifetime in the presence of 1 bar (100%) oxygen. It shows that PtTFPP in AP200/19 shows the highest $\Delta\tau_{0.05\%} = 62.53 \pm 3.66\%$ and therefore is the most suitable for ultra-low detection

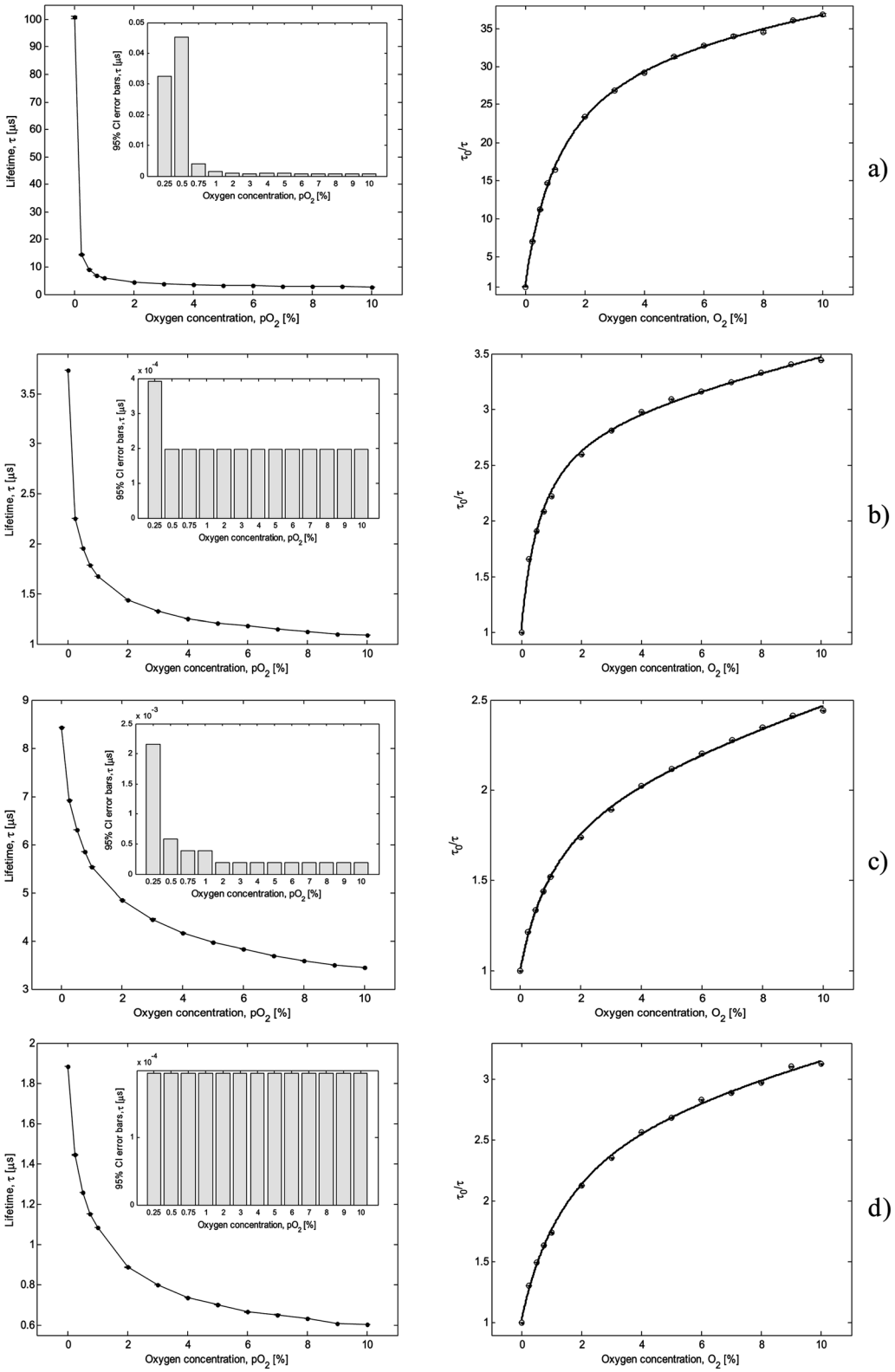

Fig. 3 Calibration curves of (a) PtTFPP, (b) N969, (c) N1008 and (d) EB146 incorporated into AP200/19 at 21 °C. Left, decay time plots. Right, Stern–Volmer plots. Each point in figures represents the average value of 100 luminescence-lifetime measurements together with its error (*i.e.*, $\bar{\tau} \pm$ error); where $\bar{\tau} = (1/100)\sum_{n=1}^{N=100} \tau_n$, and error bars indicate the 95% confidence intervals based on Student's *t*-distribution, calculated as: error (95% CI) $= 1.96s/\sqrt{N}$; with $s = \left((1/N-1)\sum_{i=1}^{N=100}(\tau_i - \bar{\tau})^2\right)^{1/2}$ (standard deviation of the $N = 100$ luminescence-lifetime measurements).

Table 2 Oxygen sensitivity of dye-AP200/19 films between 0–1% and 0–10% O_2

		Dye[a]			
Range	Parameter	PtTFPP	N969	N1008	EB146
0–1% O_2	K_{SV1} (bar^{-1})	3102 ± 132	941 ± 194	401 ± 51	289 ± 73
	x_1	0.99 ± 0.02	0.54 ± 0.05	0.26 ± 0.04	0.52 ± 0.04
	K_{SV2} (bar^{-1})	0.00 ± 0.00	15.19 ± 7.61	20.14 ± 3.59	7.92 ± 5.84
	x_2	0.03 ± 0.01	0.45 ± 0.05	0.73 ± 0.04	0.47 ± 0.04
	R^2	0.9988 ± 0.0016	0.9999 ± 0.0001	0.9997 ± 0.0004	0.9997 ± 0.0005
0–10% O_2	K_{SV1} (bar^{-1})	2568 ± 614	479 ± 72	145 ± 32	170 ± 19
	x_1	0.90 ± 0.10	0.64 ± 0.01	0.52 ± 0.01	0.64 ± 0.01
	K_{SV2} (bar^{-1})	1.66 ± 0.83	2.22 ± 0.44	2.35 ± 0.14	1.83 ± 0.70
	x_2	0.02 ± 0.00	0.33 ± 0.01	0.46 ± 0.01	0.33 ± 0.01
	R^2	0.9994 ± 0.0008	0.9983 ± 0.0005	0.9992 ± 0.0001	0.9985 ± 0.0009

[a] [Dye concentration] = 1.5 mg mL^{-1}; the results are the average of 3 replicas $\pm s\frac{t}{\sqrt{n}}$ ($n = 3$, $t = 4.303$ ($2P = 0.05$)).

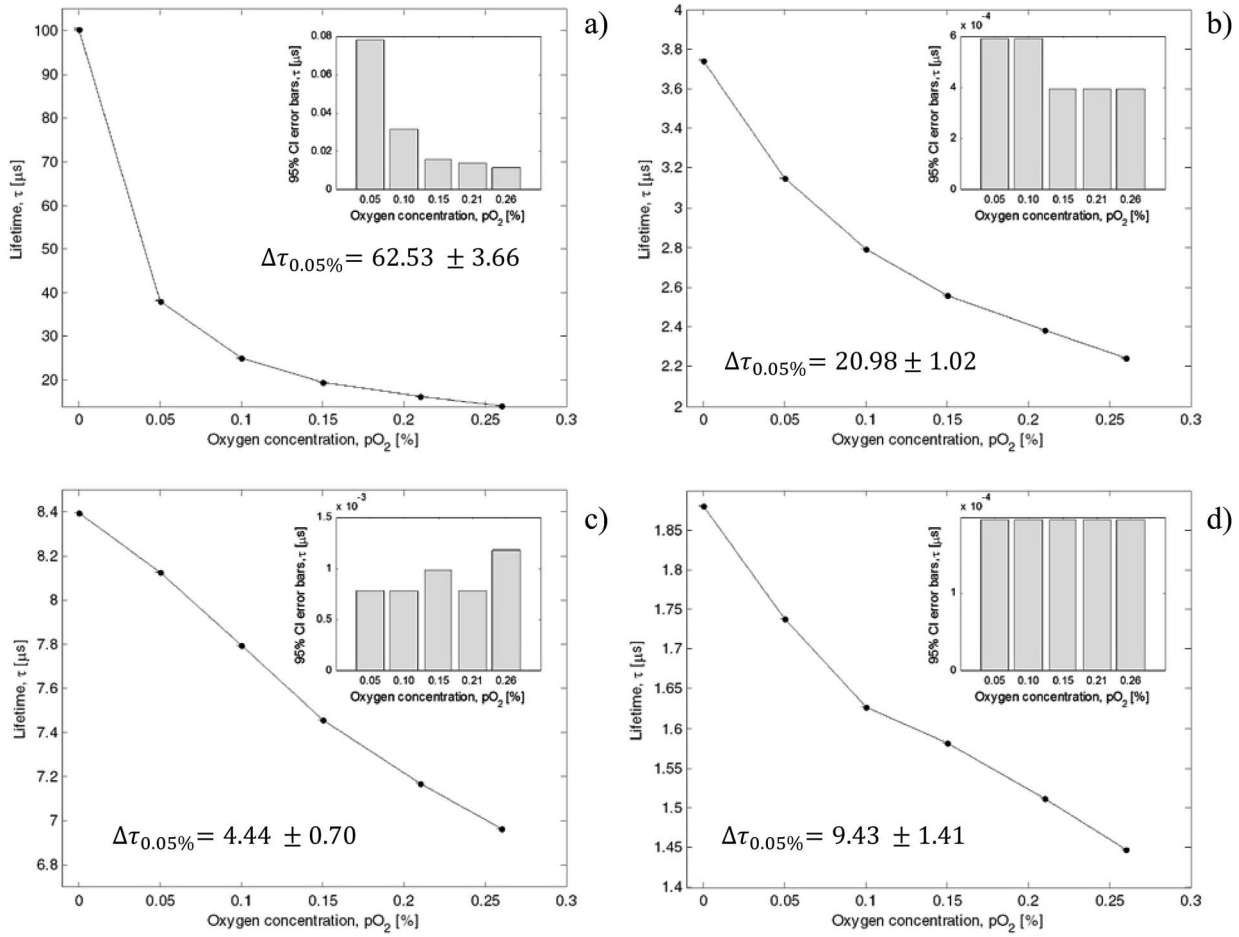

Fig. 4 Variation of the luminescence lifetime between 0 and 0.26% pO_2 of (a) PtTFPP, (b) N969, (c) N1008 and (d) EB146 incorporated into AP200/19 at 21 °C and the parameter $\Delta\tau_{0.05\%}$. Each point in figures represents the average value of 100 luminescence-lifetime measurements together with its error (*i.e.*, $\bar{\tau} \pm$ error); where $\bar{\tau} = (1/100)\sum_{n=1}^{N=100}\tau_n$, and error bars indicate the 95% confidence intervals based on Student's *t*-distribution, calculated as: error (95% CI) $= 1.96s/\sqrt{N}$; with $s = \left((1/N-1)\sum_{i=1}^{N=100}(\tau_i - \bar{\tau})^2\right)^{1/2}$ (standard deviation of the $N = 100$ luminescence-lifetime measurements).

of oxygen. It means that the 62.53% of the signal of the sensing phase is quenched at 0.05% O_2. The most sensitive Ir(III) complex-based nanocomposite between 0 and 0.05% O_2 is N969 incorporated into AP200/19, which shows a $\Delta\tau_{0.05\%}$ value of 20.98 ± 1.02%.

Finally, to demonstrate the usefulness of the developed sensing films, several air samples were analysed and the oxygen concentrations measured with the sensing films are compared with the real O_2 concentration in Table 3.

Table 4 Response times (t_{95}) of the dyes incorporated into AP200/19[a]

	t_{95} Response time (s)	
Dye	0–10% pO_2	10–0% pO_2
PtTFPP	24.5 ± 0.5	44.0 ± 0.8
N969	18.3 ± 0.4	47.3 ± 0.4
N1008	7.6 ± 0.4	20.7 ± 0.3
EB146	18.0 ± 0.4	37.9 ± 0.4

[a] [Dye concentration] = 1.5 mg mL^{-1}; the results are the average of 3 replicas $\pm s\frac{t}{\sqrt{n}}$ ($n = 3$, $t = 4.303$ ($2P = 0.05$)).

Reversibility, response times, stability and the effect of humidity

The physico-chemical quenching reaction does not consume oxygen and therefore is a reversible process. Fig. 2 shows the variation of the phase-shift *versus* the partial pressure of oxygen; when the membranes are consecutively exposed to 0 and 100% O_2, the phase-shift sensing responses are completely reversible. The complete reversibility of the luminescence lifetime of the oxygen-sensitive films allows the continuous monitoring of increased and decreased pO_2 levels.

The oxygen-sensitive membranes show short response times: the t_{95} response times for all of the sensing films are shown in Table 4. All of them were shorter than 24 s when changing from 0 to 100 vol% pO_2, and shorter than 47 s when changing from 100 to 0 vol% pO_2. In comparison with other membranes, the registered response times are higher. For example, PtTFPP incorporated into PS shows a response time of 18 s when changing from 0 to 100 vol% pO_2 and 60 s when changing from 100 to 0 vol% pO_2;[56] when incorporated into polytrifluoroethylmethacrylate, PtTFPP shows a response time of 5.6 s when changing from 0 to 100 vol% pO_2 and 32 s when changing from 100 to 0 vol% pO_2.[50] The registered response times are in fact the response time of the system, which is the time needed by the system to change the O_2 concentration from 0 to 100% and reverse. This claim is corroborated by the response times determined for these dyes immobilised into the same nanostructured solid support measured by intensity which were determined to be lower than 2 s when changing from 0 to 10 vol% pO_2 and lower than 4 s when changing from 10 to 0 vol% pO_2.[30]

An important concern common to all optical sensors is the degradation of the sensor's quantum efficiency following prolonged sampling and continuous illumination. Thus, to evaluate the optical stability of the sensing films, they were illuminated with the LED over a period of 2 h, which corresponds to 7200 measuring points, as one second is enough to acquire a single point. The data corresponding to the variation of the phase shift and the amplitude of the emitted sinusoidal waveform were recorded for different oxygen concentrations at the same time. Amplitude is correlated with the luminescent intensity of the sensing film; therefore this parameter will determine if the lifetime measurements are more stable than the intensity ones. Fig. 5 shows the results for PtTFPP and N969 as examples of this study; see ESI (Fig. ESI-7†) for the other sensing films. The amplitude (or intensity) of PtTFPP immobilized into AP200/19 decreases by 12.8 mV (corresponding to an error of 3.75% over the full-scale range of the sensing film) when the film is illuminated for 2 h. On the other hand, the phase shift decreases by only 0.1 degrees (corresponding to an error of 0.16% over the full-scale range of the sensing film). Similar results were obtained for the other sensing films: N1008 decreases by 46 mV (8.25% error) in amplitude and 0.89 degrees (2.67% error) in phase shift, N969 decreases by 184 mV (24.05% error) in amplitude and 1.56 degrees (3.97% error) in phase shift, and EB146 decreases by 192 mV (27.79% error) in amplitude and 1.45 degrees (4.41% error) in phase shift. Thus, the phase-based measurement of the luminescence lifetime is less affected by photobleaching than the intensity-based measurement over the two hours test period (see Fig. 5). This result is promising in improving the applicability and long-term stability of the optical sensing film, and thus strongly supports the selection of phase-based lifetime as the preferred sensing technique.

Table 3 Measurement capability of the developed sensing films

	Determined pO_2; % (relative error; %)			
Real pO_2; %	PtTFPP-AP200/19	N969-AP200/19	N1008-AP200/19	EB146-AP200/19
0.10	0.101 (1.22)	0.098 (1.67)	0.102 (2.34)	0.104 (3.46)
0.21	0.206 (1.92)	0.205 (2.52)	0.217 (3.21)	0.204 (2.70)
0.50	0.492 (1.62)	0.497 (2.43)	0.508 (3.20)	0.505 (3.67)
0.75	0.769 (2.50)	0.751 (2.07)	0.763 (2.97)	0.737 (2.67)
1	0.979 (2.07)	0.997 (1.89)	0.997 (3.13)	0.999 (2.78)
2	2.025 (1.27)	1.9652 (2.11)	1.929 (3.55)	2.053 (3.40)
5	5.025 (1.27)	5.074 (2.24)	5.039 (3.55)	5.046 (3.30)
8	7.840 (1.99)	8.100 (2.85)	8.155 (3.50)	7.751 (3.11)

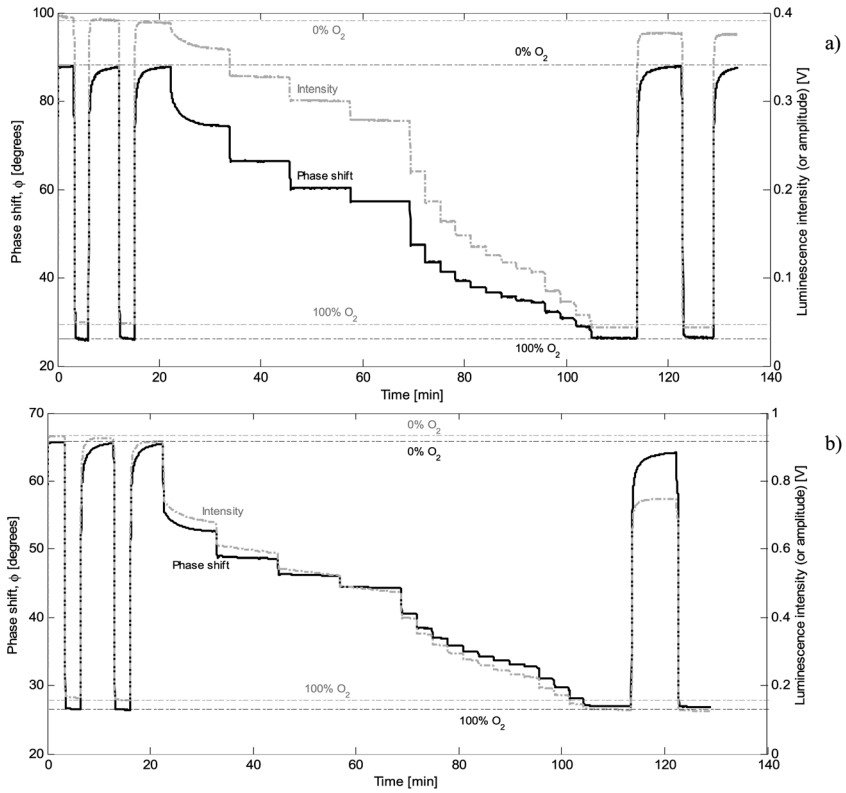

Fig. 5 Stability of the phase shift (dark bold line) and amplitude (doted light line) of (a) PtTFPP and (b) N969 incorporated into AP200/19 at 21 °C.

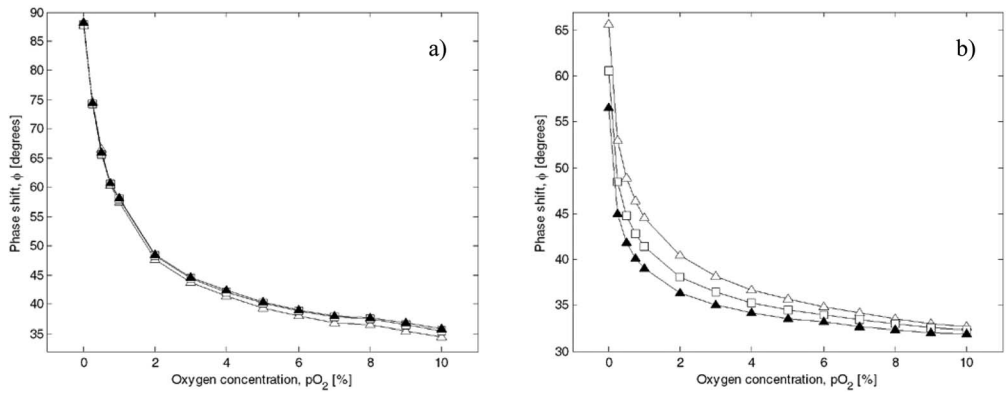

Fig. 6 Effect of relative humidity (△0% RH, □ 20% RH and ▲ 80% RH) on the phase shift of (a) PtTFPP and (b) N969 incorporated into AP200/19 at 21 °C.

Since their analytical performance (K_{SV}) did not change over 12 months stored under ambient conditions and in the absence of light, the long-term stability of all the oxygen-sensitive membranes is considered to be sufficiently good for measurements in the gas phase.

Finally, these dyes have not been immobilised into a hydrophobic membrane therefore the effect of the humidity on the sensing response has to be evaluated in order to demonstrate their real capability. PtTFPP and N969 immobilised into AP200/19 have been used to determine the concentration of oxygen between 0 and 100% at several relative humidities (0, 10, 20, 40, 60 and 80% RH). ESI (see Tables ESI-22 to ESI-25†) and Fig. 6 show the experimental results. It is possible to conclude that PtTFPP immobilised into AP200/19 is not affected by RH. On the other hand, N-969 immobilised into AP200/19 is highly affected by RH as an increase of the RH results in a decrease of the sensitivity. Therefore, if N-969 is used, the relative humidity of the media has to be taken into account in the calibration of the sensing film.

Conclusion

The luminescent platinum-complex PtTFPP and iridium-complexes N969, N1008 and EB146 were investigated for the

optical sensing of low and ultra-low oxygen concentrations using phase-shift measurements. The organometallic complexes were incorporated into a nanostructured, metal oxide matrix and characterized under a controlled atmosphere.

To the best of our knowledge, this is the first time that a Pt(II) complex has been incorporated into AP200/19. The spectral properties of PtTFPP are not affected by the solid support but, interestingly, its luminescence lifetime increases significantly ($\tau_{0\ (AP200/19)} = 97$ μs, $\tau_{0\ (PS)} = 55$ μs and $\tau_{0\ (silica\ beads)} = 71$ μs). This sensing film also shows the highest sensitivity, with a Stern–Volmer constant equal to 3102 ± 132 bar^{-1} in the range between 0 and 1% O_2 and 2568 ± 614 bar^{-1} in the range between 0 and 10% O_2. When compared to PtTFPP immobilized in polystyrene, the Stern–Volmer constant is over 62 times higher in the range 0–10% O_2 for PtTFPP immobilized in AP200/19. In comparison to PtTFPP immobilized on silica beads, the sensitivity of PtTFPP incorporated into AP200/19 improved more than 8 times in the range 0–1% O_2. In addition, this O_2-sensing film is not affected by humidity even though AP200/19 is not a hydrophobic membrane. Concerning the Ir(III) doped films, the most sensitive one is based on N969, which shows a Stern–Volmer constant of 941 ± 194 bar^{-1} in the range between 0 and 1% O_2 and 479 ± 72 bar^{-1} in the range between 0 and 10% O_2. Thus, N969 incorporated into AP200/19 shows a sensitivity about 23 times higher than that of PfTFPP immobilized into PS and more than 2 times higher than that of PtTFPP immobilized on silica beads. Therefore, N969 is a possible alternative to the PtTFPP complex for oxygen trace sensing with a different emitted wavelength.

In order to demonstrate that these sensing films can be used for ultra-low oxygen detection, the gas station was modified in order to decrease the amount of oxygen to 0.05%. The variation of the phase shift between 0 and 0.26% demonstrates this claim and the parameter $\Delta\tau_{0.05\%}$ shows that the most sensitive sensing film for controlling ultra-low oxygen concentrations (lower than 0.05% O_2) consists of PtTFPP incorporated into AP200/19, with a $\Delta\tau_{0.05\%}$ value of 62.53 ± 3.66%. These results make this film one of the most sensitive sensing films published in the literature. It was followed by the incorporation of N969 into AP200/19 ($\Delta\tau_{0.05\%}$ value of 20.98 ± 1.02%), further supporting its use as an alternative to PtTFPP with a different emitted wavelength.

The photostability study proved the high stability of the proposed sensing films and demonstrated that the phase-based measurement of the luminescence lifetime minimizes the effect of photobleaching of the optical sensing films, which significantly improves their applicability.

Finally, the oxygen-sensitive films show complete reversibility with short response times and long-term stability of more than 12 months.

Acknowledgements

The authors gratefully acknowledge the financial support from the Spanish Ministry of Economy and Competitiveness (CTQ2011-25316 and Medina-Rodríguez's grant reference BES-2009-026919) and the Regional Government of Andalusia (Excellence projects P07-FQM-2625 and P07-FQM-2738). Also, the authors are grateful to Ilford Imaging Switzerland GmbH (Switzerland) for supplying the metal oxide membranes.

References

1 J. Janata, M. Josowicz, P. Vanýsek and D. M. DeVaney, *Anal. Chem.*, 1998, **70**, 179R–208R.
2 D. B. Papkovsky and T. C. O'Riordan, *J. Fluoresc.*, 2005, **15**, 569–584.
3 J. F. Fernández-Sánchez, T. Roth, R. Cannas, M. K. Nazeeruddin, S. Spichiger, M. Graetzel and U. E. Spichiger-Keller, *Talanta*, 2007, **71**, 242–250.
4 J. R. Lakowicz, *Principles of Fluorescence Spectroscopy*, Kluwer Academic, New York, 2nd edn, 1999.
5 S. M. Borisov, A. S. Vasylevska, C. Krause and O. S. Wolfbeis, *Adv. Funct. Mater.*, 2006, **16**, 1536–1542.
6 S. M. Borisov, R. Seifner and I. Klimant, *Anal. Bioanal. Chem.*, 2011, **400**, 2463–2474.
7 K. Koren, S. M. Borisov, R. Saf and I. Klimant, *Eur. J. Inorg. Chem.*, 2011, 1531–1534.
8 Y. Amao, *Microchim. Acta*, 2003, **143**, 1–12.
9 O. S. Wolfbeis, *J. Mater. Chem.*, 2005, **15**, 2657–2669.
10 C. McDonagh, C. S. Burke and B. D. MacCraith, *Chem. Rev.*, 2008, **108**, 400–422.
11 O. S. Wolfbeis, *Anal. Chem.*, 2008, **80**, 4269–4283.
12 S. M. Mitrovski and R. G. Nuzzo, *Lab Chip*, 2005, **5**, 634–645.
13 S. M. Borisov, P. Lehner and I. Klimant, *Anal. Chim. Acta*, 2011, **690**, 108–115.
14 R. Loloee, P. A. Askeland and R. N. Ghosh, *Proceedings of IEEE Sensors*, 2007.
15 C. A. K. Lange, P. Stavrakas, U. F. O. Luhmann, D. J. De Silva, R. R. Ali, Z. J. Gregor and J. W. B. Bainbridge, *Am. J. Ophthalmol.*, 2011, **152**, 406–412.
16 A. L. Medina-Castillo, J. F. Fernández-Sánchez and A. Fernández-Gutiérrez, *Adv. Funct. Mater.*, 2011, **21**, 3488–3495.
17 K. Xie, X.-W. Zhang, L. Huang, Y.-T. Wang, Y. Lei, J. Rong, C.-W. Qian, Q.-L. Xie, Y.-F. Wang, A. Hong and S. Xiong, *Cytotechnology*, 2011, **63**, 345–350.
18 D. H. Song, H. D. Kim and K. C. Kim, *Opt. Lasers Eng.*, 2012, **50**, 74–81.
19 G. A. Holst, T. Köster, E. Voges and D. W. Lübbers, *Sens. Actuators, B*, 1995, **29**, 231–239.
20 O. Ergeneman, G. Dogangil, M. P. Kummer, J. J. Abbott, M. K. Nazeeruddin and B. J. Nelson, *IEEE Sens. J.*, 2008, **8**, 29–37.
21 D. E. Achatz, R. J. Meier, L. H. Fischer and O. S. Wolfbeis, *Angew. Chem., Int. Ed.*, 2011, **50**, 260–263.
22 W. Trettnak, C. Kolle, F. Reininger, C. Dolezal and P. O'Leary, *Sens. Actuators, B*, 1996, **36**, 506–512.
23 M. Tscherner, C. Konrad, A. Bizzarri, M. Suppan, M. Cajlakovic and V. Ribitsch, *IEEE Sens. J.*, 2009, 1660.
24 F. A. Rainey and A. Oren, in *Methods in Microbiology*, ed. F. A. Rainey and A. Oren, Elsevier, 2006, vol. 35, pp. 1–25.
25 R. C. Soliva-Fortuny and O. Martin-Belloso, *Trends Food Sci. Technol.*, 2003, **14**, 341–353.

26 E. V. D. B. Vilas-Boas and A. A. Kader, *Postharvest Biol. Technol.*, 2006, **39**, 155–162.
27 J. R. Gorny, B. Hess-Pierce, R. A. Cifuentes and A. A. Kader, *Postharvest Biol. Technol.*, 2002, **24**, 271–278.
28 S. C. Fonseca, F. A. R. Oliveira, J. K. Brecht and K. V. Chau, *Postharvest Biol. Technol.*, 2005, **35**, 279–292.
29 M. Marín-Suárez, B. F. E. Curchod, I. Tavernelli, U. Rothlisberger, R. Scopelliti, I. Jung, D. Di Censo, M. Grätzel, J. F. Fernández-Sánchez, A. Fernández-Gutiérrez, M. K. Nazeeruddin and E. Baranoff, *Chem. Mater.*, 2012, **24**, 2330–2338.
30 M. Marín-Suárez del Toro, J. F. Fernández-Sánchez, E. Baranoff, M. K. Nazeeruddin, M. Gräetzel and A. Fernández-Gutiérrez, *Talanta*, 2010, **82**, 620–626.
31 M. I. J. Stich, L. H. Fischer and O. S. Wolfbeis, *Chem. Soc. Rev.*, 2010, **39**, 3102–3114.
32 S. M. Borisov and I. Klimant, *Anal. Chem.*, 2007, **79**, 7501–7509.
33 A. L. Medina-Castillo, J. F. Fernández-Sánchez, C. Klein, M. K. Nazeeruddin, A. Segura-Carretero, A. Fernández-Gutiérrez, M. Graetzel and U. E. Spichiger-Keller, *Analyst*, 2007, **132**, 929–936.
34 J. F. Fernández-Sánchez, R. Cannas, S. Spichiger, R. Steiger and U. E. Spichiger-Keller, *Anal. Chim. Acta*, 2006, **566**, 271–282.
35 Y. Amao and I. Okura, *J. Porphyrins Phthalocyanines*, 2009, **13**, 1111–1122.
36 Y. Amao, K. Asai, I. Okura, H. Shinohara and H. Nishide, *Analyst*, 2000, **125**, 1911–1914.
37 Y. Amao, T. Miyashita and I. Okura, *Analyst*, 2000, **125**, 871–875.
38 Y. Amao, T. Miyashita and I. Okura, *React. Funct. Polym.*, 2001, **47**, 49–54.
39 J. F. Fernández-Sánchez, I. Fernández, R. Steiger, R. Beer, R. Cannas and U. E. Spichiger-Keller, *Adv. Funct. Mater.*, 2007, **17**, 1188–1198.
40 J. F. Fernández-Sánchez, T. Nezel, R. Steiger and U. E. Spichiger-Keller, *Sens. Actuators, B*, 2006, **113**, 630–638.
41 K. Tsukada, S. Sakai, K. Hase and H. Minamitani, *Biosens. Bioelectron.*, 2003, **18**, 1439–1445.
42 J. Dakin and B. Culshaw, *Optical Fiber Sensors: Applications, Analysis and Future Trends*, Artech House, Norwood, MA, 1997.
43 S. Medina-Rodríguez, A. de la Torre-Vega, J. F. Fernández-Sánchez and A. Fernández-Gutiérrez, *Sens. Actuators, B*, 2013, **176**, 1110–1120.
44 T. S. Yeh, C. S. Chu and Y. L. Lo, *Sens. Actuators, B*, 2006, **119**, 701–707.
45 M. A. Chan, J. L. Lawless, S. K. Lam and D. Lo, *Anal. Chim. Acta*, 2000, **408**, 33–37.
46 C. McDonagh, C. Kolle, A. K. McEvoy, D. L. Dowling, A. A. Cafolla, S. J. Cullen and B. D. MacCraith, *Sens. Actuators, B*, 2001, **74**, 124–130.
47 P. Hartmann, M. J. P. Leiner and M. E. Lippitsch, *Sens. Actuators, B*, 1995, **29**, 251–257.
48 D. Andrzejewski, I. Klimant and H. Podbielska, *Sens. Actuators, B*, 2002, **84**, 160–166.
49 F. De Angelis, S. Fantacci, N. Evans, C. Klein, S. M. Zakeeruddin, J. E. Moser, K. Kalyanasundaram, H. J. Bolink, M. Graetzel and M. K. Nazeeruddin, *Inorg. Chem.*, 2007, **46**, 5989–6001.
50 Y. Amao, T. Miyashita and I. Okura, *J. Fluorine Chem.*, 2001, **107**, 101–106.
51 M. Schäferling, *Angew. Chem., Int. Ed.*, 2012, **51**, 3532–3554.
52 A. S. Kocincova, S. M. Borisov, C. Krause and O. S. Wolfbeis, *Anal. Chem.*, 2007, **79**, 8486–8493.
53 R. C. Evans and P. Douglas, *ACS Appl. Mater. Interfaces*, 2009, **1**, 1023–1030.
54 Y. Feng, J. Cheng, L. Zhou, X. Zhou and H. Xiang, *Analyst*, 2012, **137**, 4885–4901.
55 X. D. Wang, H. X. Chen, Y. Zhao, X. Chen and X. R. Wang, *TrAC, Trends Anal. Chem.*, 2010, **29**, 319–338.
56 S. K. Lee and I. Okura, *Anal. Commun.*, 1997, **34**, 185–188.
57 V. I. Ogurtsov and D. B. Papkovsky, *Sens. Actuators, B*, 1998, **51**, 377–381.
58 S. Nagl, C. Baleizão, S. M. Borisov, M. Schäferling, M. N. Berberan-Santos and O. S. Wolfbeis, *Angew. Chem., Int. Ed.*, 2007, **46**, 2317–2319.